

# A Magnetar Strength Surface Magnetic Field for the Slowly Spinning Down SGR 0418+5729

Tolga Güver<sup>1\*</sup>, Ersin Göğüş<sup>2</sup>, & Feryal Özel<sup>1</sup>

<sup>1</sup>*Department of Astronomy, University of Arizona, 933 N. Cherry Ave., Tucson, AZ 85721*

<sup>2</sup>*Sabanci University, Faculty of Engineering and Natural Sciences, Orhanlı– Tuzla, İstanbul, 34956 Turkey*

15 January 2013

## ABSTRACT

The observed upper bound on the spin down rate of the otherwise typical Soft Gamma-ray Repeater SGR 0418+5729 has challenged the interpretation of this source as a neutron star with ultrastrong magnetic fields. Current limits imply a dipole magnetic field strength of less than  $7.5 \times 10^{12}$  G (Rea et al. 2010), which is significantly smaller than that of a typical SGR. Independent of the properties inferred from X-ray timing, the X-ray spectra of neutron stars allow a measurement of their magnetic field strengths because they are distorted from pure blackbodies due to the presence of a magnetic field in a radiative equilibrium atmosphere. In this paper, we model high signal-to-noise XMM-Newton spectra of SGR 0418+5729 to place constraints on the strength of the magnetic field at the surface of the neutron star. Our analysis shows that neutron star atmosphere models with moderate magnetic field strengths ( $10^{12-13}$  G) cannot fit the X-ray spectra, whereas, models with stronger magnetic fields are able to account for the observations. We find that the strength of the magnetic field at the surface is  $1.0 \times 10^{14}$  G. This value, although lower than all of the other SGRs analyzed to date, is still high enough to generate the observed X-ray bursts from the source. In connection to the spindown limits, it also implies a significantly non-dipolar structure of the magnetic field. We discuss the results of our spectral modeling and compare them with other SGRs.

**Key words:** stars: neutron - X-ray: individual: SGR 0418+5729

## 1 INTRODUCTION

Soft Gamma-ray Repeaters (SGRs) are neutron stars that are identified by the repeated bursts they emit in hard X-rays and soft gamma-rays. During their burst active phases, SGRs emit anywhere from a few to thousands of short bursts, typically lasting a fraction of a second. Energy released during such a short time is very large, ranging from  $\sim 10^{37}$  erg to  $10^{40}$  erg. On rare occasions, SGRs emit extremely energetic giant flares, lasting for a few hundreds of seconds and releasing a total energy in excess of  $10^{44}$  erg (Palmer et al. 2005).

SGRs also display persistent bright X-ray emission with luminosities of the order of  $L_X \lesssim 10^{35}$  erg s<sup>−1</sup>, which significantly exceeds the spindown power that can be generated by these slowly rotating neutron stars. Both the persistent X-ray emission and the energetic bursts led to the interpretation of SGRs as extremely magnetized neutron stars, or magnetars (Duncan & Thompson 1992; see Woods & Thompson 2006 for a detailed review). Within the magnetar paradigm,

the decay of a very strong magnetic field ( $10^{14} - 10^{15}$  G) powers the persistent emission from SGRs (Thompson & Duncan 1996), while the observed bursts are attributed either to cracking of the neutron crust that is strained by magnetic stress (Thompson & Duncan 1995) or to magnetic reconnection (Lyutikov 2003).

Large period derivatives, of the order of  $\dot{P} \simeq 10^{-11}$  s s<sup>−1</sup> measured from numerous SGRs in the past indicated large inferred dipole spindown fields  $B_{\text{dip}} = 10^{14} (P/5\text{s})^{1/2} (\dot{P}/10^{-11} \text{s s}^{-1})^{1/2}$  G, thus lending further support to the magnetar character of these sources (e.g., Kouveliotou 1998). When models of high magnetic field neutron star atmospheres and magnetospheres were used to fit to the continuum X-ray spectra of magnetars, these analyses also yielded magnetic field strengths that are comparable to the inferred dipole fields with a typical range of  $2 - 5 \times 10^{14}$  Gauss (e.g., Güver et al. 2007, 2008; Özel, Güver, & Göğüş 2008; Ng et al. 2010; Göğüş et al. 2011).

The ubiquitous presence of large period derivatives in SGRs is now being challenged by the unusually small period derivative measured in SGR 0418+5729. Early attempts to obtain its period derivative, and therefore, to establish its

\* E-mail: tguver@email.arizona.edu

inferred dipolar magnetic field strength, were inconclusive (Woods et al. 2009; Kuiper & Hermesen 2009; Esposito et al. 2010). Using multi-satellite observations spanning over 440 days following the onset of the outburst from this source, Rea et al. (2010) recently reported a  $2\sigma$  upper limit to the period derivative, implying that the inferred dipolar magnetic field strength of SGR 0418+5729 should be less than  $7.5 \times 10^{12}$  G.

SGR 0418+5729 is a regular SGR in every other way and a transient magnetar candidate (Rea & Esposito 2011): It was discovered on 2009 June 5 by emitting two bursts detected with GBM on board Fermi Gamma-ray Space Telescope (van der Horst et al. 2010). The energy released by these two events were modest, totaling  $8 \times 10^{36}$  erg and  $4 \times 10^{37}$  erg in the 20–200 keV band. Rossi X-ray Timing Explorer observations of the source following the discovery revealed the 9.07 s spin period (Göğüş et al. 2009). Detectors on board Swift, Fermi, and RXTE have allowed a growing number of transient magnetars to be discovered in the recent years, which are first detected via bursting activity and accompanied persistent flux increase up to several orders of magnitude. Persistent flux of these transient sources decreases back to quiescent level ( $\approx 10^{-13}$  erg cm $^{-2}$  s $^{-1}$ ) on a time scale of months to years (Rea & Esposito 2011). X-ray output variation of SGR 0418+5729 also very much resembles that of transient magnetar candidates: the 1–10 keV flux rapidly increased in conjunction with bursting and subsequently decayed by a factor of 10 over a time span of  $\sim 150$  days (Esposito et al. 2010). SGR 0418+5729 is located towards the Galactic anti-center and likely to be in the Perseus arm or the outer-arm of our Galaxy with a distance of  $\approx 2$  kpc or higher (van der Horst et al. 2010).

In this paper, we aim to place constraints on the magnetic field strength of SGR 0418+5729 using X-ray spectroscopy. To this end, we analyze the high signal-to-noise X-ray spectrum of SGR 0418+5729 obtained from XMM-Newton observations. We use a number of different X-ray spectral models to constrain the physical properties of the neutron star. In particular, we employ (i) the phenomenological blackbody plus power-law model that has been traditionally used to fit SGR spectra, (ii) the low-to-moderate magnetic field Neutron Star Atmosphere model, or NSA (Pavlov et al. 1995; Zavlin, Pavlin, & Shibano 1996), and (iii) the high magnetic field Surface Thermal Emission and Magnetospheric Scattering (STEMS) model (Güver, et al. 2007, 2008). We find that the thermal spectrum of SGR 0418+5729 is best described by high magnetic field model. We also compare the magnetic field determined spectroscopically to the dipole magnetic field inferred from spindown. Because the spectroscopically determined field probes the strength measured on the neutron star surface, whereas the dipole field is the one inferred at the light cylinder, this comparison can be revealing for the field geometry of SGR 0418+5729.

We introduce the XMM-Newton data and our data reduction procedure in the next section. In §3, we fit the spectrum with the three different continuum models. Finally, we discuss the implications of the inferred surface magnetic field strength and compare our findings for this source with those of SGRs in general to address the possible differences between them in the final section.

## 2 OBSERVATIONS AND DATA ANALYSIS

In the period following its discovery through its X-ray/soft-gamma-ray bursts, SGR 0418+5729 could not be observed immediately with pointing telescopes due to its unfavorable sky location. In particular, Swift XRT observations of the source could start about a month after the discovery, while the XMM-Newton observation was performed about two months after. Because the X-ray intensity of the source steadily declined following the outburst (see Figure 1 of Esposito et al. 2010), only the large collecting area of XMM-Newton was able to provide sufficiently high quality X-ray spectrum for the measurement of spectral parameters. We, therefore, use in this study the archival XMM-Newton observation that took place on 2009 August 12 (Obs ID. 0610000601). We note that SGR 0418+5729 was still not in quiescence during the XMM-Newton observation (Esposito et al. 2010). During this observation, the source count-rate as observed with the EPIC-pn and MOS detectors were, 1.35 and 0.5 c s $^{-1}$ , respectively. EPIC-pn and MOS detectors were operated in small and partial window modes with time resolutions of 6 and 300 ms, respectively, to prevent photon pile-up.

Part of the XMM-Newton observation, especially towards the end, was severely affected by large particle flares. We are, therefore, able to use  $\approx 36$  ks out of the total exposure time of 65 ks. We utilize data collected with both the EPIC-pn and EPIC-MOS cameras.

We used the *epproc* and *emproc* tasks for the EPIC-pn and EPIC-MOS data with the Science Analysis Software (SAS) version 10.0.0 and the latest available calibration files as of December 2010. We extracted X-ray spectra using a circular region with a radius of 32 arc-seconds centered on the source. Similarly, background regions were selected from a source free region with a typical radius of 50 arc-second. We used the *rmfgen* and *arfgen* tools to create response and ancillary response files. We rebinned the X-ray spectra to have at least 30 counts per bin and not to oversample the intrinsic energy resolution of the detectors by more than a factor of 3.

## 3 X-RAY SPECTRAL ANALYSIS AND RESULTS

We fit the data with XSPEC version 12.5.1n (Arnaud, 1996). In all the fits, we used the *tbabs* model and the ISM abundances (Wilms et al. 2000) to account for the effects of interstellar absorption. The XMM-Newton Calibration team reported that the EPIC-MOS detectors measure 5–8% higher fluxes than the EPIC-pn consistently over the whole energy band<sup>1</sup>. However, the exact amount of this excess flux varies over different energy ranges. Therefore, in all our fits we allowed the normalization parameters of the models to be free between the detectors and added a 1% systematic uncertainty to take into account the possible energy dependence of the uncertainties in instrumental calibrations. We calculated the unabsorbed flux using the *cflux* model in XSPEC. Because of the above-mentioned calibration uncertainty, we only report the flux and/or emitting area values as measured

<sup>1</sup> see, e.g., <http://xmm.vilspa.esa.es/docs/documents/CAL-TN-0018.pdf>.

with EPIC-pn. We assumed a gravitational redshift for the neutron star as 0.25, corresponding to a neutron star mass of  $1.4 M_{\odot}$  and radius of 11.5 km. We fit all spectra in the 0.5 to 6.5 keV energy range. Unless otherwise noted, all the uncertainties quoted are for 68% confidence interval.

We first fit the X-ray spectra using a combination of a blackbody (*bbbodyrad* as defined in XSPEC) and a power-law model. We performed this analysis only as a phenomenological classification of the source spectrum because the atmospheric structure even for a weak or “zero” magnetic field has a strong effect on the spectral shape of the X-ray emission of neutron stars and has been shown to distort it away from a blackbody (see e.g. Romani 1988; Pavlov et al. 1995). The spectrum and the best-fit model are shown in the left panel of Figure 1. Blackbody plus power-law provided a moderate fit with a  $\chi^2/\text{dof}$  of 1.12 for 346 degrees of freedom. The best fit model resulted in a hydrogen column density of  $(1.10 \pm 0.05) \times 10^{22} \text{ cm}^2$ , a blackbody temperature of  $0.93 \pm 0.006 \text{ keV}$ , and a photon index of the power-law component of  $3.18 \pm 0.19$ . The temperature is unusually high for two reasons. First, the blackbody component dominates over the power-law component at high photon energies, i.e., in the  $> 1.5 \text{ keV}$  range, as can be seen in Figure 1, which is physically difficult to interpret and is also contrary to what is seen in the spectra of other SGRs. Second, this high temperature corresponds to an extremely small emitting radius of 0.18 km/2kpc. Such a small emitting radius is especially hard to interpret given the observed pulsed fraction of 20-40% in the soft X-rays (Esposito et al. 2010).

The current constraints on the period derivative of SGR 0418+5729 point to a dipolar magnetic field strength smaller than  $7.5 \times 10^{12} \text{ G}$ . We, therefore, tried to fit the spectrum of SGR 0418+5729 with low to intermediate magnetic field strength neutron-star atmosphere models. The NSA model (Pavlov et al. 1995; Zavlin, Pavlin, & Shibano 1996) provides a model for the X-ray spectra emitted from a hydrogen atmosphere of a neutron star at three different magnetic field strengths:  $B < 10^8 - 10^9 \text{ G}$ ,  $B = 10^{12} \text{ G}$ , and  $B = 10^{13} \text{ G}$ . The fit parameters of the NSA model, in addition to the magnetic field strength, are the neutron star mass and radius, the surface temperature, and the normalization, which is a function of the source distance  $1/D_{\text{kpc}}^2$ .

We consider the  $B < 10^8 \text{ G}$  case only for completeness, because it would be unfeasible to account for the X-ray pulsations observed from SGR 0418+5729 if indeed possessed a negligible magnetic field. For this case, the NSA model does not provide a good fit with a  $\chi^2/\text{dof}$  equal to 1.29 for 350 degrees of freedom and yields a best-fit surface temperature of 0.73 keV ( $8.5 \times 10^6 \text{ K}$ ). As with the blackbody-plus-power-law fit, this rather high temperature corresponds to a very small best fit normalization of  $3.0 \times 10^{-10}$ , or equivalently an emitting radius of  $R = 0.4 \text{ km}/2 \text{ kpc}$ .

At a field strength of  $B = 10^{12} \text{ G}$ , the NSA model cannot fit the spectrum of SGR 0418+5729, yielding a minimum  $\chi^2/\text{dof} = 13.88$  for 350 degrees of freedom. The surface temperature also hits  $10^7 \text{ K}$ , which is the maximum of the allowed range in the models. Finally, the obtained best fit normalization of  $8.5 \times 10^{-11}$  translates to an unphysically small emitting radius of  $R = 0.21 \text{ km}/2 \text{ kpc}$ . This indicates that the spectrum of SGR 0418+5729 is inconsistent with a surface magnetic field strength that is comparable to its dipole field strength inferred from its period derivative.

We performed a final NSA fit where we set the magnetic field strength to  $B = 10^{13} \text{ G}$ . The quality of the fit improved compared to the  $10^{12} \text{ G}$  case but is still not adequate, yielding a  $\chi^2/\text{dof} = 3.88$  for 350 degrees of freedom. The best-fit temperature again hits the upper limit of the allowed range at  $10^7 \text{ K}$  (0.86 keV), corresponding to a normalization of  $1.3 \times 10^{-10}$ , which is an emitting radius of  $R = 0.3 \text{ km}/2 \text{ kpc}$ .

In an attempt to obtain statistically better fits and to investigate whether additional spectral components would have an effect on the measured effective temperature values, we also modeled the X-ray spectrum of SGR 0418+5729 with an absorbed NSA plus a power-law model. We found that the addition of the power-law component statistically improved the fits, yielding  $\chi^2/\text{dof}$  values of 1.13, 2.78, and 1.49 for 346 degrees of freedom, when the magnetic field strength was set to 0,  $10^{12}$ , and  $10^{13} \text{ G}$ , respectively. However, the addition of the power-law component did not decrease the inferred effective temperature, resulting in values that still reached the upper temperature limit of the model. In the right panel of Figure 1, we show the X-ray spectra and an example case for the NSA+PL models, where the strength of the magnetic field was set to  $10^{12} \text{ G}$ .

We finally modeled the spectrum of SGR 0418+5729 with magnetar strength fields in the few  $\times 10^{13} - 10^{15} \text{ G}$  range, which may reflect the higher multipole field strengths present at the stellar surface. To this end, we used the Surface Thermal Emission and Magnetospheric Scattering model (STEMS, see Güver et al. 2007, 2008). STEMS takes into account the effects of the ultrastrong magnetic fields on the fully ionized hydrogen atmospheres of magnetars (Özel 2001, 2003) and the resonant cyclotron scattering of the surface photons by mildly relativistic charges in the magnetosphere (Lyutikov & Gavril 2006). For the calculation of the surface emission, we follow Özel (2001, 2003) and solve the radiative transfer equations in a polarization-mode-dependent manner including the absorption, emission and scattering processes in the atmosphere. We also take into account the effects of vacuum polarization resonance and include the interaction of photons with protons in the plasma, which gives rise to absorption features at the proton cyclotron energy (Özel 2003). In the stellar magnetosphere, we incorporate a treatment of resonant cyclotron scattering, following Lyutikov & Gavril (2006). Resonant cyclotron scattering can take place in a neutron star magnetosphere as long as there is a sufficient density of moderately relativistic electrons and the resulting up-scattering shifts the initial spectrum to higher energies and smears out the proton cyclotron features (Lyutikov & Gavril 2006).

In the STEMS model, we use the emission emerging from the surface as input for the resonant cyclotron scattering model to obtain the resulting energy distribution of photons. In total STEMS depends on four parameters: the surface effective temperature ( $kT = 0.1 - 0.6 \text{ keV}$ ), the strength of the magnetic field at the surface ( $B = 0.6 - 50 \times 10^{14} \text{ G}$ ), the optical depth to scattering in the magnetosphere ( $\tau = 1.0 - 12.0$ ), and the velocity of the particles in the magnetosphere ( $\beta = 0.1 - 0.7$ ). Note that, even though in the calculations of Lyutikov & Gavril (2006), a high optical depth is motivated by a twist angle, this is not a necessary assumption. Such high charge densities are seen in the magnetospheres of even normal pulsars and the only differ-

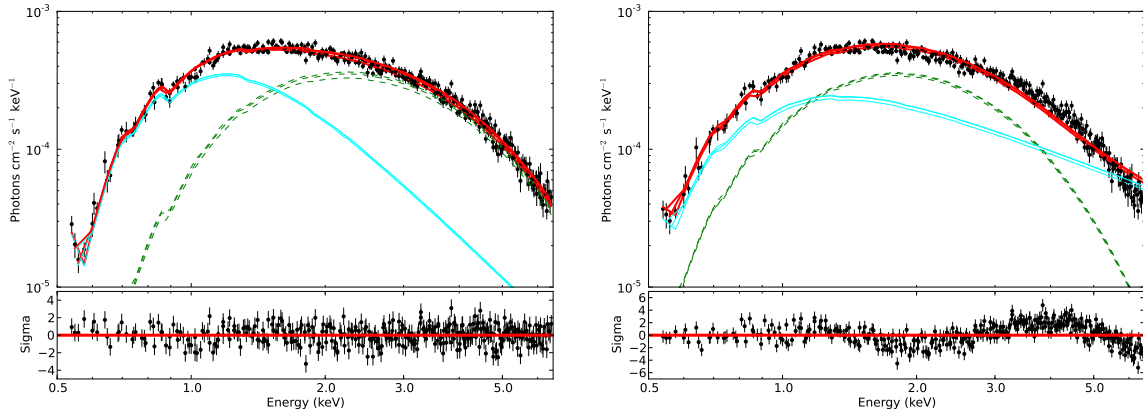


**Figure 1.** Best fit fluxed blackbody + power-law (upper left panel) and neutron star atmosphere (NSA) + power-law (upper right panel) fit to the X-ray spectrum of SGR 0418+5729 obtained with the XMM-Newton. The magnetic field strength in the NSA model is set to  $10^{12}$  G. Blackbody + power-law provides a moderate fit with  $\chi^2/\text{dof} = 1.12$  for 346 degrees of freedom, while the NSA + power-law is a poor fit with  $\chi^2/\text{dof} = 2.78$  for 346 degrees of freedom. In both cases, the thermal component dominates (shown with dashed green lines) over the power-law component (shown with thick cyan lines) at high photon energies, i.e., in the  $> 1.5$  keV range, which is difficult to interpret physically. Lower panels show the residuals from each fit, respectively.

ence between the SGR 0418+5729 and a neutron star with a magnetar-strength dipole field would be the occurrence of the resonant layers closer to the neutron star surface. As an example, based on the current limit on the dipole field of SGR 0418+5729, the resonant layer would be at  $4 R_{\text{NS}}$ , whereas for a quadrupole field that is  $10^{14}$  G at the surface, the resonant layer would be at  $\approx 6 R_{\text{NS}}$ . Finally we take into account general relativistic effects on the propagation of the photons by assuming a gravitational redshift.

Compared to the blackbody plus a power-law fit, STEMS model provided an equally good fit to the XMM-Newton spectrum, resulting in a  $\chi^2/\text{dof}$  of 1.18 for 347 degrees of freedom. We show the best fit model curve and the X-ray spectra in Figure 2. The parameters of the best fit model were: the surface magnetic field strength  $B = (1.00^{+0.02}_{-0.01}) \times 10^{14}$  G, the surface effective temperature  $kT = 0.246^{+0.003}_{-0.01}$  keV, the scattering optical depth in the magnetosphere  $\tau = 8.94^{+1.18}_{-0.18}$  and the particle velocity in the magnetosphere  $\beta = 0.56 \pm 0.01$ . The inferred optical depth and the average electron velocity are well within the assumptions of the resonant cyclotron scattering model (see, e.g., Section 3.4 of Lyutikov & Gavrilov 2006). We also found a hydrogen column density of  $(0.74 \pm 0.02) \times 10^{22} \text{ cm}^2$  and the unabsorbed 0.5-6.5 keV source flux as  $(8.53^{+0.05}_{-0.06}) \times 10^{-12} \text{ erg s}^{-1} \text{ cm}^{-2}$ . The inferred emitting radius corresponding to this effective temperature and flux is  $R = 2.98 \text{ km}/2 \text{ kpc}$ . We note that in this fit fractional emitting area, i.e.,  $A_{\text{hot}}/A_{\text{NS}}$ , where  $A_{\text{NS}}$  is the entire neutron star surface area, is in the right range to produce the pulsed fraction of 20-40%, as observed by Esposito et al. (2010) in the soft X-rays.

We present in Figure 3 the confidence contours of the best fit effective temperature and the magnetic field strength at the surface of the neutron star. From the confidence contours it can clearly be seen that the STEMS model provides a lower limit to the surface magnetic field strength of the neutron star of  $\approx 1 \times 10^{14}$  G. Because our focus in this paper is the surface magnetic field strength of SGR 0418+5729, we further explored the uncertainty in this parameter by do-

ing the following: We fit the data by freezing the magnetic field at 1000 different points within the  $0.6 - 4.0 \times 10^{14}$  G range and allowing the other parameters to vary. Figure 3 shows the variation of the  $\chi^2/\text{dof}$  over the full magnetic field range investigated. It is evident from the distinct minimum in the  $\chi^2$  in this figure that the magnetic field strength at the surface of the neutron star is uniquely constrained and is found to be  $1.0 \times 10^{14}$  G.

## 4 DISCUSSION

The recent discovery and the subsequent observations of SGR 0418+5729 have raised a number of questions on our understanding of the SGRs and AXPs, especially owing to a lack of secular evolution in its spin period. A number of explanations, both within and outside the context of the magnetar model, have been proposed to interpret the peculiarity of SGR 0418+5729. For example, the effects of a stronger toroidal magnetic field below the surface on the neutron star crust was employed to create the observed X-ray bursts independent of strength of the dipole component (see, e.g., Perna & Pons 2011; Rea et al. 2010). The existence of a fallback disk has been proposed to evolve the neutron star to its current spin period with a dipole field as low as  $10^{12-13}$  G (Alpar, Ertan, & Çalışkan 2010; see also Ertan et al. 2007).

In this paper, we analyzed the X-ray spectrum of SGR 0418+5729 to constrain its surface magnetic field strength, as well as the temperature and the magnetospheric parameters of the neutron star. We find that the empirical blackbody + power-law model provides a moderate fit, but the emitting area inferred from this fit is unphysically small ( $R = 0.18 \text{ km}/2 \text{ kpc}$ ). In addition, contrary to the physical expectations and in contrast to other AXP and SGR spectra, the blackbody component dominates over the power-law component in the higher, as opposed to the lower, energy regime. We also found that realistic atmosphere models of a neutron star with moderate magnetic field strengths

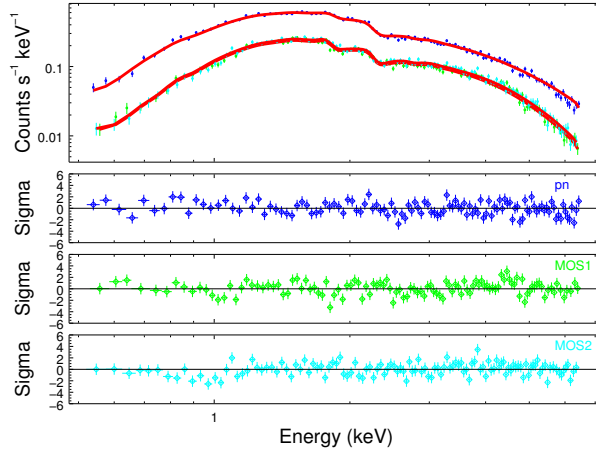


**Figure 2.** XMM-Newton EPIC-pn (blue) and EPIC-MOS (green and cyan) spectra of the SGR 0418+5729. Best fit STEMS model is also shown with red thick lines. Residuals from the model for each detector are shown in lower panels.

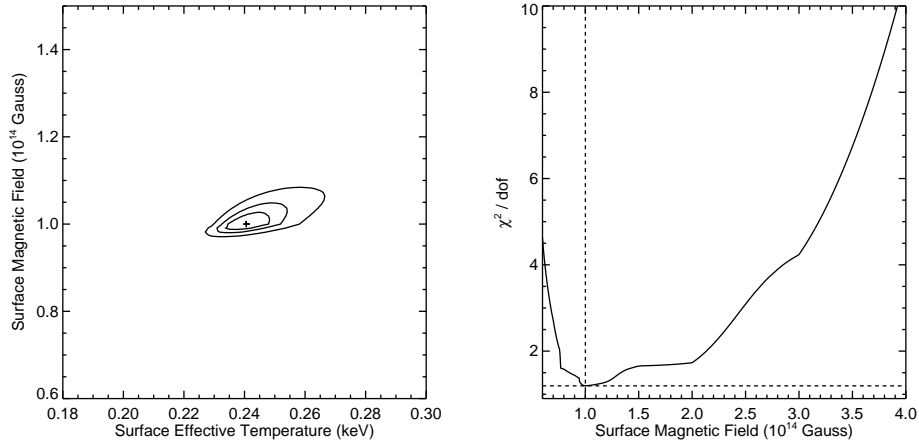


**Figure 3.** *Left Panel:* Confidence contours of the best fit surface effective temperature and the magnetic field strength at the surface of the neutron star as inferred from the STEMS model. *Right Panel:* Variation of the  $\chi^2/\text{dof}$  with the surface magnetic field strength. Horizontal and vertical dashed lines show  $\chi^2/\text{dof}$  and surface magnetic field strength for the best fit model.

(NSA), do not describe the spectrum adequately, yielding  $\chi^2/\text{dof} \geq 3.9$ . In contrast, neutron star atmosphere models with magnetar-strength fields (STEMS) produces a fit with  $\chi^2/\text{dof} = 1.18$  for 347 degrees of freedom. The best fit value of the magnetic field strength is  $1.0 \times 10^{14}$  G. Thus, the spectral analysis strongly disfavors X-ray models where the magnetic field strength at the surface is assumed to be  $10^8$ – $10^9$ ,  $10^{12}$ , or  $10^{13}$  G.

X-ray observations of a number of other magnetars have been successfully modeled with neutron star atmospheres with high magnetic field strengths, including XTE J1810–197 (Güver et al. 2007), 4U 0142+61 (Güver et al. 2008), 1E 1048.1–5937, 1RXS J170849.0–400910 (Özel et al. 2008), 1E 1547.0–5408 (Ng et al. 2011) and SGR 1900+14 (Gögüş et al. 2011), and were used to obtain the surface parameters of the neutron stars such as their magnetic field strengths and effective temperatures. The spectroscopically inferred magnetic field strength values for

these sources, in units of  $10^{14}$  G, are  $2.77 \pm 0.05$ ,  $4.75 \pm 0.03$ ,  $2.26 \pm 0.05$ ,  $3.96 \pm 0.17$ ,  $3.1 \pm 0.5$ , and  $5.0 \pm 0.48$ , respectively. In Figure 4, we compare these spectroscopically determined field strengths with the previously reported inferred dipole magnetic field for each source, which we obtained from the McGill SGR/AXP Catalog<sup>2</sup>, Ng et al. (2011), and Özel et al. (2008). For all of these sources, the spectrally inferred surface magnetic field strength is in good agreement with dipole magnetic field estimates, differing at most by a factor of four. SGR 0418+5729 is the first magnetar candidate for which the surface magnetic field strength is significantly larger than the limit on the dipole magnetic field ( $\geq 15$  times larger). It is also interesting that the surface magnetic field strength we report here for SGR 0418+5729 is the low-

<sup>2</sup> <http://www.physics.mcgill.ca/pulsar/magnetar/main.html>

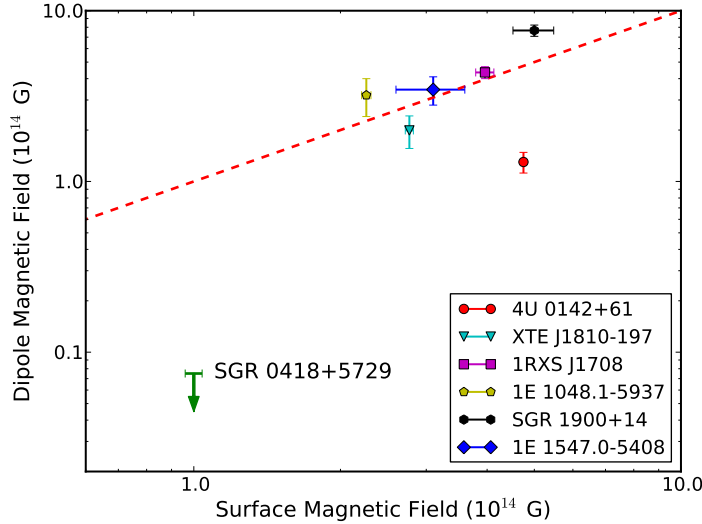


**Figure 4.** Comparison of the magnetic field strengths as inferred using the STEMS model to the dipole fields deduced from the spindown properties for seven magnetar candidates. The error bars in dipole field strengths represent the range of measured spindown rates for each source, while the error bars in the spectroscopic magnetic field strength represent  $2\text{-}\sigma$  statistical uncertainties. Dashed lines show the relation where  $B_{surf} = B_{dip}$ .

est among other STEMS measurements for other AXPs and SGRs so far.

Even though the dipole field strengths inferred from spindown involve a number of simplifying assumptions, relaxing them in realistic simulations leads to a factor of two difference in the inferred magnetic field strengths (Contopoulos & Spitkovsky 2006). Therefore, the discrepancy between the field strength inferred from the spindown of SGR 0418+5729 and the field strength inferred from both its spectrum and its bursts is too large to be accounted for in this way. Instead, the difference points to a complex magnetic field geometry, i.e, it can be attributed to the presence of higher order multipole components at the surface of the neutron star, which can shape the characteristics of the X-ray emission but do not contribute to the spindown. The multipole fields are likely to play a role in determining the pulse shapes observed in AXPs and SGRs (Özel 2002). In this interpretation, the higher order components of the magnetic field can also cause the fracturing of the neutron star crust, leading to the observed X-ray bursts. Further comparisons of the surface and dipole magnetic field strengths of AXPs and SGRs, as well as numerical simulations of the magnetic field evolution in young neutron stars may help further constrain the magnetic field strengths and geometries of X-ray bright neutron stars.

## ACKNOWLEDGMENTS

We thank the anonymous referee for his/her comments that improved the clarity of the manuscript. This work makes use of observations obtained with XMM-Newton, an ESA science mission with instruments and contributions directly funded by ESA Member States and NASA. F. Ö. and T. G. acknowledge support from NSF grant AST-07-08640.

## REFERENCES

- Alpar M. A., Ertan Ü., Çalışkan Ş., 2011, *ApJ*, 732, L4
- Arnaud K. A., 1996, *ASPC*, 101, 17
- Contopoulos I., Spitkovsky A., 2006, *ApJ*, 643, 1139
- Duncan R. C., Thompson C., 1992, *ApJ*, 392, L9
- Ertan Ü., Erkut M. H., Ekşi K. Y., Alpar M. A., 2007, *ApJ*, 657, 441
- Esposito P., et al., 2010, *MNRAS*, 405, 1787
- Göğüş E., Woods P., Kouveliotou C., 2009, *ATel*, 2076, 1
- Göğüş E., Güver T., Özel F., Eichler D., Kouveliotou C., 2011, *ApJ*, 728, 160
- Güver T., Özel F., Göğüş E., Kouveliotou C., 2007, *ApJ*, 667, L73
- Güver T., Özel F., Göğüş E., 2008, *ApJ*, 675, 1499
- Kouveliotou C., et al., 1998, *Natur*, 393, 235
- Kuiper L., Hermesen W., 2009, *ATel*, 2151, 1
- Lyutikov M., 2003, *MNRAS*, 346, 540
- Lyutikov M., Thompson C., 2005, *ApJ*, 634, 1223
- Lyutikov M., Gavril F. P., 2006, *MNRAS*, 368, 690
- Ng C.-Y., et al., 2011, *ApJ*, 729, 131
- Özel F., 2001, *ApJ*, 563, 276
- Özel F., 2002, *ApJ*, 575, 397
- Özel F., 2003, *ApJ*, 583, 402
- Özel F., Güver T., Göğüş E., 2008, *AIPC*, 983, 254
- Palmer D. M., et al., 2005, *Nature*, 434, 1107
- Pavlov G. G., Shibano Y. A., Zavlin V. E., Meyer R. D., 1995, *Ins.conf*, 71
- Perna R., Pons J. A., 2011, *ApJ*, 727, L51
- Rea N., et al., 2010, *Sci*, 330, 944
- Rea N., Esposito P., 2011, *heep.conf*, 247
- Romani R. W., 1987, *ApJ*, 313, 718
- Spitkovsky A., 2006, *ApJ*, 648, L51
- Spitkovsky A., 2008, *AIPC*, 983, 20
- Thompson C., Duncan R. C., 1995, *MNRAS*, 275, 255
- Thompson C., Duncan R. C., 1996, *ApJ*, 473, 322
- van der Horst A. J., et al., 2010, *ApJ*, 711, L1
- Wilms J., Allen A., McCray R., 2000, *ApJ*, 542, 914
- Woods P. M., Thompson C., 2006, *csxs.book*, 547
- Woods P. M., Gogus E., Kouveliotou C., et al., 2009, *ATel*, 2152,

